Synaptic and supra-synaptic organisation of the dopaminergic projection to the striatum.

Marlene E. Pfeffer[1,2,#], Marie Pronot[1,2,#], Maria-Florencia Angelo[1,2], Roman Walle[3], Fabrice P. Cordelières[4], Florian Levet[1,2,4], Stéphane Claverol[5], Sabrina Lacomme[4], Melina Petrel[4], Christelle Martin[1,2], Vincent Pitard[6], Véronique Desmedt-Peyrusse[3], Thomas Biederer[7], Pierre Trifilieff[3], and Etienne Herzog[1,2].

[1] Interdisciplinary Institute for Neuroscience, Université de Bordeaux, UMR 5297, 33000 Bordeaux, France.
[2] Interdisciplinary Institute for Neuroscience, CNRS UMR 5297, 33000 Bordeaux, France.
[3] Univ. Bordeaux, INRAE, Bordeaux INP, NutriNeuro, UMR 1286, F-33000, Bordeaux, France
[4] Bordeaux Imaging Center, Université de Bordeaux, CNRS UMS 3420, INSERM US4, 33000, Bordeaux, France.
[5] Univ. Bordeaux, Plateforme Proteome, 33000, Bordeaux, France
[6] UB'FACSility CNRS UMS 3427, INSERM US 005, Univ. Bordeaux, F-33000 Bordeaux, France
[7] Department of Neuroscience, Tufts University School of Medicine, Boston, MA 02111, USA.
[#] these authors contributed equally to the work

Correspondence should be addressed to Etienne HERZOG
etienne.herzog@u-bordeaux.fr
Université de Bordeaux
Interdisciplinary Institute for NeuroScience - UMR 5297
Centre Broca Nouvelle-Aquitaine
146 rue Léo Saignat
CS 61292 Case 130
33076 Bordeaux Cedex (FRANCE)

Highlights:

1. Fluorescence Activated Synaptosome Sorting allows for the establishment of a molecular synaptome of striatal dopaminergic projections.
2. Dopaminergic varicosities adhere to receptor filled post-synaptic membranes.
3. Dopaminergic projections build hub synapses with excitatory and inhibitory projections.
4. SynCAM 2 is a strong candidate for the adhesion and differentiation of dopamine-effector hub synapses.

SUMMARY

Dopamine transmission is a monoaminergic system involved in reward processing and motor control. Volume transmission is thought to be the main mechanism by which monoamines modulate effector transmission though synaptic structures are scarcely described. Here, we applied a fluorescence activated synaptosome sorting workflow to dopaminergic projections to the striatum and explored cellular and molecular features of the dopaminergic synaptome. This demonstrated that dopaminergic varicosities adhere to post-synaptic membrane baring cognate receptors. We further identified a specific bond of varicosities to glutamatergic or GABAergic synapses in structures we named dopaminergic "hub synapses". Finally, we showed that the synaptic adhesion protein SynCAM 2 is strongly expressed at dopaminergic hub synapses. Our data strongly suggest that neuromodulation frequently operates from hub-synapses on local receptors, presumably in conjunction with extra-synaptic volume transmission. We provide a new framework for the molecular exploration of dopaminergic synapses and more generally on discrete synapse populations ex-vivo.

ACKNOWLEDGMENT

Our work benefited from the excellent technical support from the central facilities at Bordeaux university: Bordeaux Imaging Center (CNRS UMS 3420, INSERM US4); Biochemistry and Biophysics of Proteins; Flow cytometry UB'FACSility (CNRS UMS 3427, INSERM US5); animal care & breeding; Genotyping; proteomics. We thank Niels Christian Danbolt for the kind gift of antibodies. We are grateful to François Georges, André Callas, Nicolas Heck, Peter Vanhoutte and David Perrais for fruitful discussions. Elisabeth Normand, Melissa Deshors provided an excellent support for surgeries and animal care. This study benefited from the the Agence Nationale de la Recherche consortium fundings (IDEX Bordeaux ANR-10-IDEX-03-02 ; Labex BRAIN ANR-10-LABX-43 BRAIN ; France Bio Imaging ANR-10-INBS-04) as well as funding to PT and EH (ANR-10-LABX-43 BRAIN Dolipran) and funding to PT (ANR-16-CE16-0022 SynLip), and funding to TB (National Institutes of Health R01 DA018928). EH received funding from Fondation pour la Recherche Médicale (ING20150532192). RW holds a fellowship from the French ministry of research.

INTRODUCTION

Since the 1950's with the first ultrastructural characterization of the synapse in the central nervous system (Gray, 1959) a wide variety of synapse types have been described based on morphological criteria (Harris, n.d.). The archetypal synapse type extensively studied is the asymmetric excitatory synapse on dendritic spines (Gray, 1959) whose ultrastructure is easily identifiable in the tissue and routinely studied *in vitro* using primary neuronal cultures (Banker and Cowan, 1977). Alternatively, symmetric synapses are mostly inhibitory or modulatory. They do not display post-synaptic densities and are more difficult to identify *in situ* (Descarries et al., 1996; Moss and Bolam, 2008). Moreover, many types of synaptic organizations are not abundant enough and/or accessible in *in vitro* models. These limitations hinder our understanding of neuronal network functioning.

While glutamate and GABA (Gamma-Amino Butyric Acid) neurotransmissions drive point to point information locally, modulatory neurotransmitters pace regional activity through volume transmission in the neuropil (Agnati et al., 1995; Greengard, 2001). Dopamine transmission is a main neuro-modulation system involved in several functions such as movement initiation, reward prediction error and incentive processes, notably by its projections onto medium spiny neurons (MSN) of the striatum (Kreitzer, 2009). Dopamine signalling is presumed to modulate glutamate transmission onto MSNs through release of dopamine mainly from varicosities devoid of synaptic differentiation while a minority forms synapses onto MSN spines or dendrites, as well as presynapses (Bamford et al., 2004; Descarries et al., 1996; Moss and Bolam, 2008). However, recent work challenges the model of volume dopamine transmission by providing intriguing evidence for local point-to-point signalling. In fact, optophysiology approaches revealed rapid and local transmission at dopaminergic projections to the striatum (Howe and Dombeck, 2016; Pereira et al., 2016; Yagishita et al., 2014), which is in accordance with the requirement for synaptic vesicle

release machinery for fast dopamine release at striatal varicosities (C. Liu et al., 2018). Moreover, the distribution of varicosities in the striatal neuropil appears biased toward proximity with the surrounding effector synapses (Moss and Bolam, 2008), and dopamine receptors interact physically and functionally with glutamate and GABA receptors (Cahill et al., 2014; Cepeda and Levine, 2012; Ladépêche et al., 2013b; F. Liu et al., 2000), suggesting a tight coupling between dopamine and effector transmissions.

In the present work we aimed to unravel the cellular and molecular synaptome of single projection pathways (Zhu et al., 2018). This can critically complement current connectomic approaches using optophysiology and tracing methods, which are limited in terms of molecular analysis of specific synapses at play in a given circuit (Schreiner et al., 2016). To that end, we established a workflow combining fluorescence tracing of the dopaminergic pathway, fluorescence activated synaptosome sorting and an array of semi-quantitative analysis methods ranging from conventional immunofluorescence characterization to mass spectrometry-based proteomics. With this approach we provide the first ex-vivo model to analyse thoroughly the cellular and molecular organisation of dopaminergic synapses from mouse striatum. This new model unravels the existence of a physical coupling between dopaminergic and effector synapses in a complex we name “hub synapses”. Synaptic hubs may represent key units in the modulatory action of dopamine on glutamate and GABA signalling.

RESULTS

Fluorescence activated synaptosome sorting (FASS) enrichment of dopaminergic synaptosomes reveals synaptic hub structures.

Here we labelled the Dopaminergic projection onto the striatum using the Dopamine Transporter promoter-cre transgenic mouse line (Turiault et al., 2007) and a viral vector providing cre-dependent conditional expression of EGFP in neurons (Oh et al., 2014) (Figure

1A1-2). We miniaturized the classical sucrose synaptosome fractionation to 1.5ml tubes (De-Smedt-Peyrusse et al., 2018; Whittaker, 1993) (Figure 1A3). Fluorescence activated synaptosome sorting (FASS) allowed strong enrichment of dopaminergic varicosities together with adherent compartments (Biesemann et al., 2014; Luquet et al., 2016) (Figure 1A4, B & C, and S1). We finally established a set of recovery and analysis methods (semi-quantitative immunofluorescence, super-resolution microscopy, electron microscopy and Mass Spectrometry) that allows answering several key questions regarding the cellular and molecular organization of this projection pathway (Figure 1A5-6). FASS allowed for the enrichment of DAT-EGFP labelled synaptosomes (Figure 1BC). Our gating strategy was adapted from previous work (Biesemann et al., 2014) in order to avoid sorting aggregated particles (Figure S1). Sucrose synaptosomes from DAT-EGFP tracings contained on average 3.9% singlet EGFP positive synaptosomes (3.9% ± 0.52; n=9; Figure 1C) upon reanalysis in the cell sorter after FASS EGFP synaptosomes represented around 50% of the total (49% ± 2.3%; N=9 sorts; Figure 1C). Other populations in the synaptosome samples were depleted accordingly (Figure 1C). We first explored FASS samples using transmitted electron microscopy (Figure 1D-G). We easily identified synaptosome profiles with resealed presynaptic elements (Figure 1D) and in some cases a clear adhesion with a post-synaptic membrane. Surprisingly, we also identified a significant proportion of profiles displaying several presynaptic profiles organized around possible post-synaptic membranes (Figure 1E-G). In many occurrences, the profiles were cut with an angle that prevented clear identification of all synaptic elements (Figure 1F). On another example, we found 2 distinct presynapses, one electron dense terminal with many synaptic vesicles adhering to a presynaptic element with fewer vesicles and to another compartment that could be dendritic (Figure 1E). Finally, a post-synaptic element displayed adhesion to 3 different “boutons”, one of them displaying a clearer background and less vesicles (Figure 1G). These complex micro-

structures were preserved even though our procedure exposed the tissue to shearing forces during homogenization and further shearing forces are applied to particles in the nozzle of the cell sorter, indicating strong adhesive interactions (see workflow in Figure 1A). We named these structures "hub synapses" and pursued our characterization to identify their molecular nature.

DAT-EGFP FASS synaptosomes display pre- and post-synaptic features of dopaminergic synapses.

What is the molecular makeup of these biochemically isolated hub synapses? We addressed this by immunostaining both FASS-sorted and unsorted singlet synaptosomes using a battery of synaptic and dopaminergic markers. Individual particles were quantified and results were plotted according to their intensity in both channels. Quadrant gates were defined to split positives and negatives for each label (see Figure 1). The top 2 quadrants are EGFP+ particles and percentages of particles are displayed in each quadrant. We first probed for the phospho-proteins Synapsin 1&2 that are found at all presynapses (De Camilli et al., 1983). Upon sorting EGFP+/synapsin+ particles representations rose from 8% before sort to 45% after sort and around 70% of EGFP labelled synaptosomes contained synapsin after sort (Figure 2B top quadrants). EGFP-/Synapsin+ synaptosomes represented 83.8% before sort and were reduced to 35.2% after sort (Figure 2A-C). A careful scrutiny using STED microscopy shows that some EGFP+ synaptosomes contain both co-localized (usually of low intensity) and apposed (usually of high intensity) synapsin labels (Figure 2D). Apposed Synapsin-rich puncta may represent glutamate or GABA presynapses.

Extending this analysis to the dopaminergic synapse content, we focused on Tyrosine Hydroxylase (TH), a marker of dopaminergic presynapses that catalyses the limiting step for dopamine synthesis (Descarries et al., 1996; Lamouroux et al., 1982; Moss and Bolam, 2008). TH positive EGFP labelled synaptosomes population rose from 54% of the total before sort to

81.7% after sort (Figure 2EF). The number of labelled particles per field of view was increased 5-fold over sorting (Figure 2G). In super-resolution, TH signals were mostly colocalized with EGFP (Figure 2H). Similarly, a strong co-localization with anti-DAT (Dopamine Transporter) signal was found. Yet, a significant number of DAT+/ EGFP- was observed that may correspond to extra synaptic axonal pieces that did not retain the cytosolic EGFP (Figure S2AB). As expected, the marker EAAT1/GLAST that labels astrocyte membranes was not associated to the EGFP-labelled synaptosomes and was depleted upon sorting (Figure S2CD). Altogether our data confirm that DAT-EGFP labelled synaptosomes display genuine dopaminergic synaptosomal markers and are strongly enriched through FASS. We then explored the co-segregation of dopamine receptors type 1 and -2 (D1R, D2R) together with DAT-EGFP labelled varicosities. D1R co-enriched nearly 10-fold with DAT-EGFP+ synaptosomes (from 3.99% to 31.8%; Figure 2IJ top right quadrants), while extra-synaptic D1R labelled particles depleted 2-fold (from 81% to 42%; Figure 2IJ bottom right quadrants). 55% of DAT-EGFP synaptosomes were labelled for D1R (EGFP+/D1R- 26.1%, EGFP+/D1R+ 31.8%; Figure 2I-K upper quadrants). Anti-D1R displayed patches of staining apposed to EGFP particles (Figure 2L). D2R labels were found on more than 80% of DAT-EGFP dopaminergic synaptosomes and co-enriched massively with EGFP (EGFP+/D2R- 12.3%, EGFP+/D2R+ 50%; Figure 2M-N upper quadrants). Extrasynaptic D2 receptors were depleted more than 2-fold over DAT-EGFP sorting (EGFP-/D2R+ 76% in unsorted vs 37.5% in sorted samples; Figure 2M-N lower right quadrants). D2R are auto- and hetero-receptors (Sesack et al., 1994), therefore, D2R found closely or more distantly apposed to EGFP labelled synaptosomes (Figure 2MNP) are likely to correspond to pre- and postsynaptic D2R, respectively. Altogether our data supports that nearly all dopaminergic synaptosomes carry a post-synaptic element equipped with cognate receptors.

Glutamatergic and GABAergic synaptosomes frequently adhere to dopaminergic synaptosomes.

To further characterize our dopaminergic sample, we initially aimed at screening for contaminations with classical glutamatergic and GABAergic markers. The vesicular glutamate transporter type 1 (VGLUT1) is expressed at excitatory cortico-striatal inputs impinging on spines of the medium spiny neurons (MSN) (Heck et al., 2015; Herzog et al., 2001; Moss and Bolam, 2008). Through DAT-EGFP FASS, EGFP-/VGLUT1+ synaptosomes were depleted 2-fold (76.5% unsorted vs 33.3% sorted; Figure 3AB lower right quadrants). Yet, a third of dopaminergic EGFP+ synaptosomes were associated with a VGLUT1 pre-synapse (EGFP+/VGLUT1- 44.3%, EGFP+/VGLUT1+ 22.4%; Figure 3B upper quadrants), and enriched 3-fold through FASS (7.56% in unsorted vs 22.4% in sorted samples; Figure 3AB upper right quadrants). VGLUT1 varicosities were apposed to EGFP varicosities at hub synaptosomes as revealed by super-resolution STED microscopy (Figure 3D).

Similarly VGLUT2 is a specific marker of excitatory thalamo-striatal inputs contacting MSNs (Herzog et al., 2001; Moss and Bolam, 2008). 12.7% of EGFP+ dopaminergic synaptosomes were found to be associated to a VGLUT2 bouton (11.5% of total, Figure 3F upper quadrants), while EGFP-/VGLUT2+ representation in the FASS sample was reduced 5-fold over unsorted synaptosomes (46.8% in unsorted vs 9.47% in sorted samples; Figure 3EF lower right quadrants). VGLUT2 varicosities were apposed to EGFP as revealed by STED microscopy (Figure 3H).

Finally, we probed for the vesicular inhibitory amino-acid transporter (VIAAT), that labels GABAergic terminals arising from all inhibitory neurons of the striatum (Sagné et al., 1997). VIAAT+/EGFP+ hub synaptosomes displayed a 5-fold enrichment through FASS (4.17% in unsorted vs 20.2% in sorted samples; Figure 3IJ upper right quadrants), while the EGFP-/VIAAT+ population was depleted more than 2-fold (69.3% in unsorted vs 26.3% in sorted

samples; Figure 3IJ lower right quadrants). As for excitatory synaptosomes, GABAergic synaptosomes were associated to 30% of the EGFP+ synaptosomes (20.2% of total, Figure 3J upper quadrants). At hub synapses, VIAAT+ signal appeared apposed to EGFP signal in STED microscopy (Figure 3L).

Hence our data show the frequent association of dopamine synapses with VGLUT1, VGLUT2 or VIAAT (VGAT) synapses supporting our earlier electron microscopy observations. To challenge our observations, we performed randomization tests on our images to ensure that the probability of co-sedimentation of separate particles at the same sites is low. Indeed, for all our datasets, random associations occurred on less than 2% of all events while we observed at least 11% for synaptic hub related associations (see Table 1). We further tested whether the reverse FASS experiment, sorting VGLUT1^{venus} cortico-striatal synaptosomes would co-purify TH or VGLUT2-labelled terminals (see Figure S3AI). As expected, TH varicosities were found massively associated to the striatal VGLUT1^{venus} synaptosomes (37.9% VGLUT1+/TH+ in sorted samples; Figure S3G upper right quadrant) but VGLUT2 synaptosomes were mostly segregated from VGLUT1^{venus} positive synaptosomes (Figure S3HI). Decisively, VGLUT2+/VGLUT1^{venus} + particles were not co-enriched through fluorescence sorting (8.71% in unsorted sample vs 5.45% in sorted synaptosomes; Figure S3HI upper right quadrants). Finally, we tested whether a presynaptic GABAergic marker VIAAT was associated to the post-synaptic inhibitory marker gephyrin in our singlet synaptosome samples. Surprisingly, we found that gephyrin+ particles were not kept associated to VIAAT+ synaptosomes (Figure S3J). This illustrates how adhesive strength may differ between synapse types and how shearing forces acting during homogenization and sorting may disrupt weak adhesion. As a final control for the specificity of hub-synaptosome adhesion, we performed a VGLUT1^{venus} FASS experiment through which we selectively sorted aggregates and performed electron microscopy on our aggregate sorted sample (Figure

S4). Upon reanalysis, sorted aggregates displayed a steep increase in the representation of small and large aggregates (Figure S4A-C). Singlets were still strongly represented in the reanalysed sample as it is common to brake-down aggregates into singlets through the shearing forces applied in the nozzle of the FACS (Figure S4A-C). Electron micrographs displayed many profiles of large particles (3-6µm in diameter) difficult to relate to identifiable features of the tissue and very different from the synaptosomes displayed in Figure 1 (Figure S4D).

Altogether, we identified the association of dopaminergic and effector synapses in synaptic hub structures that specifically adhere together and may mediate the modulatory influence of dopamine over excitatory and inhibitory synaptic signalling.

The synaptic adhesion protein SynCAM 2 is highly expressed at dopaminergic synapses.

In a quest to proteins specifically expressed at dopamine hub synapses we performed a mass-spectrometry analysis of FASS sample contents. A DAT-EGFP+ FASS sample was compared to unsorted singlets of the same sucrose preparation using state of the art LC-MS/MS protein label-free quantification. From a sample of 10 millions synaptosomes around 80 protein species could be identified in both samples among which only 2 where exclusively represented in the DAT-EGFP+ sample, namely, the dopamine transporter (Slc6a3) and the synaptic adhesion protein SynCAM 2 (*Cadm2*; Gene ID: 239857). Other typical synaptic proteins identified were not strongly differentially expressed between our dopaminergic and control samples (see Table 2 and Table S1-2). To further confirm our finding, we performed an immuno-staining against SynCAM 2 and identified that 92% of DAT+ synaptosomes display a SynCAM 2 signal (75.3% DAT+/SynCAM 2+ vs 6.32% DAT+/SynCAM 2-; Figure 4B upper quadrants). The proportion of DAT+/SynCAM 2+ synaptosomes was enriched 3-fold through FASS (28,2% in unsorted vs 75.3% in sorted samples; Figure 4AB upper right quadrants) while DAT-/SynCAM 2+ were depleted 3-fold (56.5% in unsorted vs 18.3% in

sorted samples; Figure 4AB lower right quadrants). Overall, SynCAM 2 displayed a staining pattern very similar to TH (compare with Figure 1E-G). In super-resolution, SynCAM 2 patches were visible tightly apposed to the DAT varicosities (Figure 4D). Hence we show for the first time that SynCAM 2 may be a major adhesion protein operating at dopaminergic projections.

Altogether, our immunofluorescence analysis of dopaminergic synaptosomes purified by FASS identified the association of TH, SynCAM 2, D2R, D1R, Synapsin, VIAAT, VGLUT2 and VGLUT1 ordered here by distance to the EGFP+ varicositiy. TH is colocalized and seen at an average distance equivalent to the resolution of our conventional epifluorescence setup (0.25µm), while VGLUT1 is apposed on average at 0.6µm distance from EGFP+ barycentre (see Figure 4E-F). We thus propose a model in which most dopaminergic varicosities adhere through SynCAM 2 to post-synaptic elements labelled by either D1 or D2 receptors. Beyond, a majority of dopaminergic synapses is also associated to effector synapses in synaptic hub structures clearly identified in electron microscopy (Figure 4G).

DISCUSSION

In order to unravelling specific molecular and cellular features of modulatory neurotransmission, we targeted the dopaminergic projection from substantia nigra and ventral tegmental area to the striatum with a synaptosome sorting based synaptomic approach (Biesemann et al., 2014; Zhu et al., 2018). Specificity for dopaminergic synaptosomes was validated by the enrichment for presynaptic dopaminergic markers as well as the adhesion of dopaminergic varicosities to D1R or D2R populated post-synaptic elements. Finally, dopaminergic synapses were frequently associated with glutamatergic or GABAergic synapses in structures identified in electron microscopy that we propose to name “hub synapses”. Congruently, we found the synaptic adhesion protein SynCAM 2 to be strongly

expressed at dopaminergic varicosities making it a candidate protein that supports the development of this synapse type.

Cellular organisation of dopaminergic projections to the striatum.

The nature of dopaminergic synaptic structures is the topic of a long-standing debate. Previous anatomical investigations in the field identified that the distribution of dopamine varicosities in the neuropil is biased toward a proximity to effector synapses but only a minority makes synapses with a target structure in the striatum (Descarries et al., 1996; Moss and Bolam, 2008). However, other authors reported the frequent occurrence of symmetrical synaptic contacts of dopaminergic thin axonal portions with MSNs spines or dendritic shafts (Freund et al., 1984; Gaugler et al., 2012; Groves et al., 1994). Our current dataset strongly advocates for a specific and frequent adhesion of dopaminergic axonal varicosities of rather small diameter with target structures (Figures 1 and 2IP). Indeed, around 55% of our EGFP+ varicosities displayed apposed D1R, while more that 80% displayed D2R labelling (Figures 2, 4). This is in accordance with MSNs being the main target of dopamine terminals in the striatum, with roughly half of the MSNs expressing D1 receptors (Striatonigral pathway), while the D2 receptor is expressed by the other half (Bertran-Gonzalez et al., 2010; Calabresi et al., 2014) as well as by dopaminergic and effector presynapses (Delle Donne et al., 1997; Hersch et al., 1995; Sesack et al., 1994).

Beyond, our data reveal that adhesion at the dopaminergic varicosity extends to synaptic hubs with effector synapses. We found that around a third of dopaminergic varicosities make hub synapses with cortico-striatal VGLUT1 synapses, more than a tenth associate with thalamo-striatal VGLUT2 synapses, and more than a quarter was associated to VIAAT inhibitory synapses (Figures 3 and 4G). Conversely, nearly half of VGLUT1 striatal synaptosomes were observed in hub synapses (Figure S3G). Providing that little overlap exists between those hub associations, around 75% of dopaminergic varicosities may adhere to hub synapses. Indeed,

VGLUT1 and VGLUT2 synaptosomes displayed little to no association when probed from a striatal sorting from VGLUT1^{venus} mice (Figure S3HI). Dopaminergic varicosities are clear to electrons and less populated with SVs (Freund et al., 1984; Gaugler et al., 2012). Synaptic hubs observed here, associate electron dense terminals strongly populated with SVs, to whiter varicosities much less populated with SVs (Figure 1FH). The occurrence of synaptic hubs may explain previous observations that striatal dopaminergic synaptosomes sediment faster than other synaptosomes in a linear sucrose gradient (Van der Krogt et al., 1983) and conversely, optimisations of the sucrose gradient centrifugations in our procedure should further improve the yield of dopaminergic sample isolation. Among control experiments, we observed that GABAergic synaptosomes do not retain an association to the post-synaptic scaffold protein gephyrin (Figure S3J). Hence, it is likely that synaptic hubs built with inhibitory synapses comprise axo-axonic contacts of dopaminergic projections to GABAergic terminals. Such profile is visible on our electron microscopy data (Figure 1F). It remains to understand whether large varicosities that are not engaged in adhesion are maintained in the process of synaptosome preparation, and whether these large varicosities are important for neurotransmission. Further investigations will be necessary to unravel whether synaptic hub formation is a structural invariant common to all sub-divisions of the striatum, and whether the proportion of hub synapses of different kinds is equivalent in all regions and physiological states.

Functional consequences of the existence of Dopaminergic synaptic hubs.

Our dataset suggest that nearly all dopaminergic terminals adhere to a post-synaptic element populated with cognate receptors. Yet, around 2/3 of the dopaminergic varicosities are thought to be “silent” at a given time in the striatum (C. Liu et al., 2018; Pereira et al., 2016). It thus seems like the formation of a synaptic contact at dopaminergic varicosity is not

sufficient to establish a functional release site but rather additional plasticity may be required to engage silent dopaminergic synapses into dopamine transmission.

The discovery of synaptic hubs linking dopaminergic and effector synapses provides a unique ex-vivo paradigm to study the complex interactions of receptors – through signalling crosstalk or heteromeric interactions - identified in the past decades (Cahill et al., 2014; Cepeda and Levine, 2012; Ladépêche et al., 2013a; F. Liu et al., 2000). As previously published, we found that many D1R or D2R labelled particles were extra-synaptic (Caillé et al., 1996; Sesack et al., 1994). Yet, most EGFP labelled synaptosomes displayed an apposed D1R or D2R. Therefore, the question is raised regarding the co-recruitment of glutamate or GABA receptors with dopamine receptors at synaptic hubs and the plasticity of this recruitment upon reward-based learning and in pathologic processes. The isolation of synaptic hubs using our approach will be ideal to monitor this plasticity. Indeed, the relationship between the status of dopamine release (active versus silent) and the recruitment of cognate hetero-receptors and auto-receptors will be important to establish using our sample preparation.

Beyond, D1R and D2R interactions with effector ionotropic receptors, Adenosine, cannabinoid, metabotropic glutamate receptors and muscarinic receptors are also important players of the striatal integration of cortical and thalamic inputs. Downstream targets of signalling such as ionic channels may also take part to the critical scaffolds at play (Calabresi et al., 2014; Surmeier et al., 2007). Thus, FASS synaptosomes will be a powerful tool to identify key molecular signalling complexes for dopamine action on striatal networks.

Synaptic adhesion at dopaminergic synaptic hubs.

Our first molecular characterization of FASS dopaminergic synaptosomes identifies the synaptic adhesion protein SynCAM 2 (Biederer, 2006; Biederer et al., 2002; Fogel et al., 2007) as a major component of the dopaminergic synapse. Indeed, SynCAM 2 mRNA is highly expressed in VTA and SNc areas of the rodent brain (Lein et al., 2007). SynCAM 2

was also reported to populate axons (Pellissier et al., 2007). We therefore propose that SynCAM 2 is part of an axonal adhesion complex responsible for the formation of dopaminergic synapses with MSNs and hub synapses with effector moieties. SynCAM 2 is thought to engage in heterophilic interactions with SynCAM1 and -4 (Fogel et al., 2007; Thomas et al., 2008). Interestingly, SynCAM 1 is a player of cocaine-induced synaptic plasticity in the striatum (Giza et al., 2013) and SynCAM 2 regulates food intake and energy balance (Yan et al., 2018), two phenomena directly related to the dopaminergic system(Tellez et al., 2016; 2013). Besides, SynCAM1 is thought to be preferentially acting at the post-synapses to induce presynaptic adhesion (Czöndör et al., 2013; D. K. Fowler et al., 2017). Hence, SynCAM1 and -2 are strong candidates to mediate adhesion through heterophilic interaction at dopamine synapses. Moreover, our data raise the possibility that SynCAM 2 has synapse-type specific roles in the development of dopaminergic hub synapses.

A previous contribution suggested that adhesion at dopaminergic synapses occur through neuroligin 2 (Uchigashima et al., 2016). Our small-scale mass spectrometry data did not identify neuroligin 2 as enriched in dopaminergic synaptosomes, but this may be due to a lower expression of neuroligin 2 compared to SynCAM 2 or DAT. Yet the action of neuroligin 2 is preeminent at inhibitory synapses (Poulopoulos et al., 2009; Varoqueaux et al., 2004). In the context of synaptic hubs, the role of neuroligin 2 may be important for the association with inhibitory synapses. Finally, additional players are certainly also important and further investigations will be important to clarify the complete machinery responsible for synaptic hub formation and maintenance.

Altogether, our work paves the way for a better understanding of dopaminergic synaptic transmission in physiology and pathology (Blumenstock et al., 2019). Future developments will allow a more thorough multi-omics (Hafner et al., 2019; Poulopoulos et al., 2019) analysis of dopaminergic samples prone to unravelling important key molecular signatures of

dopamine hub synapses. More generally, results from our study and the work of Apostolo and colleagues (Apóstolo et al., 2019) on mossy fibre terminals of the hippocampus show that FASS synaptomics is a powerful tool for the exploration of projection-specific synaptomes (Grant, 2019; Zhu et al., 2018).

REFERENCES

Agnati, L.F., Zoli, M., Strömberg, I., Fuxe, K., 1995. Intercellular communication in the brain: wiring versus volume transmission. Neuroscience 69, 711–726.

Apóstolo, N., Smukowski, S.N., Vanderlinden, J., Condomitti, G., Rybakin, V., Bos, ten, J., Portegies, S., Vennekens, K.M., Gounko, N.V., Wierda, K.D., Savas, J.N., de Wit, J., 2019. Mapping the cell-surface proteome underlying hippocampal mossy fiber synapse identity. BioRxiv 846816. doi:10.1101/846816

Bamford, N.S., Zhang, H., Schmitz, Y., Wu, N.-P., Cepeda, C., Levine, M.S., Schmauss, C., Zakharenko, S.S., Zablow, L., Sulzer, D., 2004. Heterosynaptic dopamine neurotransmission selects sets of corticostriatal terminals. Neuron 42, 653–663.

Banker, G.A., Cowan, W.M., 1977. Rat hippocampal neurons in dispersed cell culture. Brain Res 126, 397–342. doi:10.1016/0006-8993(77)90594-7

Bertran-Gonzalez, J., Hervé, D., Girault, J.-A., Valjent, E., 2010. What is the Degree of Segregation between Striatonigral and Striatopallidal Projections? Front. Neuroanat. 4. doi:10.3389/fnana.2010.00136

Biederer, T., 2006. Bioinformatic characterization of the SynCAM family of immunoglobulin-like domain-containing adhesion molecules. Genomics 87, 139–150. doi:10.1016/j.ygeno.2005.08.017

Biederer, T., Sara, Y., Mozhayeva, M., Atasoy, D., Liu, X., Kavalali, E.T., Südhof, T.C., 2002. SynCAM, a synaptic adhesion molecule that drives synapse assembly. Science 297, 1525–1531. doi:10.1126/science.1072356

Biesemann, C., Grønborg, M., Luquet, E., Wichert, S.P., Bernard, V., Bungers, S.R., Cooper, B., Varoqueaux, F., Li, L., Byrne, J.A., Urlaub, H., Jahn, O., Brose, N., Herzog, E., 2014. Proteomic screening of glutamatergic mouse brain synaptosomes isolated by fluorescence activated sorting. EMBO J 33, 157–170. doi:10.1002/embj.201386120

Blumenstock, S., angelo, M.F., Peters, F., Dorostkar, M.M., Ruf, V.C., Luckner, M., Crux, S., Slapakova, L., Arzberger, T., Claverol, S., Herzog, E., Herms, J., 2019. Early defects in translation elongation factor 1α levels at excitatory synapses in α-synucleinopathy. Acta Neuropathol. doi:10.1007/s00401-019-02063-3

Cahill, E., Pascoli, V., Trifilieff, P., Savoldi, D., Kappes, V., Luscher, C., Caboche, J., Vanhoutte, P., 2014. D1R/GluN1 complexes in the striatum integrate dopamine and glutamate signalling to control synaptic plasticity and cocaine-induced responses. Mol. Psychiatry 19, 1295–1304. doi:10.1038/mp.2014.73

Caillé, I., Dumartin, B., Bloch, B., 1996. Ultrastructural localization of D1 dopamine receptor immunoreactivity in rat striatonigral neurons and its relation with dopaminergic innervation. Brain Res 730, 17–31. doi:10.1016/0006-8993(96)00424-6

Calabresi, P., Picconi, B., Tozzi, A., Ghiglieri, V., Di Filippo, M., 2014. Direct and indirect pathways of basal ganglia: a critical reappraisal. Nat Neurosci 17, 1022–1030. doi:10.1038/nn.3743

Cepeda, C., Levine, M.S., 2012. Dopamine-NMDA receptor interactions: twenty years later. Dev. Neurosci. 34, 2–4. doi:10.1159/000338590

Cetin, A., Komai, S., Eliava, M., Seeburg, P.H., Osten, P., 2006. Stereotaxic gene delivery in the rodent brain. Nat Protoc 1, 3166–3173. doi:10.1038/nprot.2006.450

Czöndör, K., Garcia, M., Argento, A., Constals, A., Breillat, C., Tessier, B., Thoumine, O., 2013. Micropatterned substrates coated with neuronal adhesion molecules for high-content study of synapse formation. Nat Commun 4, 2252. doi:10.1038/ncomms3252

De Camilli, P., Harris, S.M., Huttner, W.B., Greengard, P., 1983. Synapsin I (Protein I), a nerve terminal-specific phosphoprotein. II. Its specific association with synaptic vesicles demonstrated by immunocytochemistry in agarose-embedded synaptosomes. J Cell Biol 96, 1355–1373.

De-Smedt-Peyrusse, V., Darriet, L., Trifilieff, P., Herzog, E., angelo, M.F., 2018. Subcellular Fractionation of Brain Tissue from Small Tissue Explants., in: Murphy, K.M. (Ed.), Synaptosomes. Humana Press, New York, NY, New York, pp. 75–84. doi:10.1007/978-1-4939-8739-9_5

Delle Donne, K.T., Sesack, S.R., Pickel, V.M., 1997. Ultrastructural immunocytochemical localization of the dopamine D2 receptor within GABAergic neurons of the rat striatum. Brain Res 746, 239–255.

Descarries, L., Watkins, K.C., Garcia, S., Bosler, O., Doucet, G., 1996. Dual character, asynaptic and synaptic, of the dopamine innervation in adult rat neostriatum: a quantitative autoradiographic and immunocytochemical analysis. J Comp Neurol 375, 167–186. doi:10.1002/(SICI)1096-9861(19961111)375:2<167::AID-CNE1>3.0.CO;2-0

Fogel, A.I., Akins, M.R., Krupp, A.J., Stagi, M., Stein, V., Biederer, T., 2007. SynCAMs organize synapses through heterophilic adhesion. J Neurosci 27, 12516–12530. doi:10.1523/JNEUROSCI.2739-07.2007

Fowler, D.K., Peters, J.H., Williams, C., Washbourne, P., 2017. Redundant Postsynaptic Functions of SynCAMs 1-3 during Synapse Formation. Front. Mol. Neurosci. 10, 24. doi:10.3389/fnmol.2017.00024

Fowler, J.E., n.d. The redundant discrete wavelet transform and additive noise. IEEE Signal Process. Lett. 12, 629–632. doi:10.1109/LSP.2005.853048

Freund, T.F., Powell, J.F., Smith, A.D., 1984. Tyrosine hydroxylase-immunoreactive boutons in synaptic contact with identified striatonigral neurons, with particular reference to dendritic spines. Neuroscience 13, 1189–1215. doi:10.1016/0306-4522(84)90294-X

Gaugler, M.N., Genç, Ö., Bobela, W., Mohanna, S., Ardah, M.T., El-Agnaf, O.M., Cantoni, M., Bensadoun, J.-C., Schneggenburger, R., Knott, G.W., Aebischer, P., Schneider, B.L., 2012. Nigrostriatal overabundance of α-synuclein leads to decreased vesicle density and deficits in dopamine release that correlate with reduced motor activity. Acta Neuropathol. 123, 653–669. doi:10.1007/s00401-012-0963-y

Giza, J.I., Jung, Y., Jeffrey, R.A., Neugebauer, N.M., Picciotto, M.R., Biederer, T., 2013. The synaptic adhesion molecule SynCAM 1 contributes to cocaine effects on synapse structure and psychostimulant behavior. Neuropsychopharmacology 38, 628–638. doi:10.1038/npp.2012.226

Grant, S.G.N., 2019. The Synaptomic Theory of Behavior and Brain Disease. Cold Spring Harb. Symp. Quant. Biol. doi:10.1101/sqb.2018.83.037887

Gray, E.G., 1959. Axo-somatic and axo-dendritic synapses of the cerebral cortex: an electron microscope study. J. Anat. 93, 420–433.

Greengard, P., 2001. The neurobiology of slow synaptic transmission. Science 294, 1024–1030. doi:10.1126/science.294.5544.1024

Groves, P.M., Linder, J.C., Young, S.J., 1994. 5-hydroxydopamine-labeled dopaminergic axons: three-dimensional reconstructions of axons, synapses and postsynaptic targets in rat neostriatum. Neuroscience 58, 593–604. doi:10.1016/0306-4522(94)90084-1

Hafner, A.-S., Donlin-Asp, P.G., Leitch, B., Herzog, E., Schuman, E.M., 2019. Local protein synthesis is a ubiquitous feature of neuronal pre- and postsynaptic compartments. Science 364. doi:10.1126/science.aau3644

Harris, K.M., n.d. Synapse Web [WWW Document]. synapseweb.clm.utexas.edu. URL http://synapseweb.clm.utexas.edu/harrislab.

Heck, N., Santos, Dos, M., Amairi, B., Salery, M., Besnard, A., Herzog, E., Boudier, T., Vanhoutte, P., Caboche, J., 2015. A new automated 3D detection of synaptic contacts reveals the formation of cortico-striatal synapses upon cocaine treatment in vivo. Brain Struct Funct 220, 2953–2966. doi:10.1007/s00429-014-0837-2

Hersch, S.M., Ciliax, B.J., Gutekunst, C.A., Rees, H.D., Heilman, C.J., Yung, K.K., Bolam, J.P., Ince, E., Yi, H., Levey, A.I., 1995. Electron microscopic analysis of D1 and D2 dopamine receptor proteins in the dorsal striatum and their synaptic relationships with motor corticostriatal afferents. J Neurosci 15, 5222–5237.

Herzog, E., Bellenchi, G.C., Gras, C., Bernard, V., Ravassard, P., Bedet, C., Gasnier, B., Giros, B., Mestikawy, El, S., 2001. The existence of a second vesicular glutamate transporter specifies subpopulations of glutamatergic neurons. J Neurosci 21, RC181.

Holmseth, S., Scott, H.A., Real, K., Lehre, K.P., Leergaard, T.B., Bjaalie, J.G., Danbolt, N.C., 2009. The concentrations and distributions of three C-terminal variants of the GLT1 (EAAT2; slc1a2) glutamate transporter protein in rat brain tissue suggest differential regulation. Neuroscience 162, 1055–1071. doi:10.1016/j.neuroscience.2009.03.048

Howe, M.W., Dombeck, D.A., 2016. Rapid signalling in distinct dopaminergic axons during locomotion and reward. Nature 535, 505–510. doi:10.1038/nature18942

Kreitzer, A.C., 2009. Physiology and Pharmacology of Striatal Neurons. Annu Rev Neurosci 32, 127–147. doi:10.1146/annurev.neuro.051508.135422

Ladépêche, L., Dupuis, J.P., Bouchet, D., Doudnikoff, E., Yang, L., Campagne, Y., Bézard, E., Hosy, E., Groc, L., 2013a. Single-molecule imaging of the functional crosstalk between surface NMDA and dopamine D1 receptors. Proc Natl Acad Sci USA 110, 18005–18010. doi:10.1073/pnas.1310145110

Ladépêche, L., Yang, L., Bouchet, D., Groc, L., 2013b. Regulation of dopamine D1 receptor dynamics within the postsynaptic density of hippocampal glutamate synapses. PLoS ONE 8, e74512. doi:10.1371/journal.pone.0074512

Lamouroux, A., Faucon Biguet, N., Samolyk, D., Privat, A., Salomon, J.C., Pujol, J.F., Mallet, J., 1982. Identification of cDNA clones coding for rat tyrosine hydroxylase antigen. Proc Natl Acad Sci USA 79, 3881–3885. doi:10.1073/pnas.79.12.3881

Lein, E.S., Hawrylycz, M.J., Ao, N., Ayres, M., Bensinger, A., Bernard, A., Boe, A.F., Boguski, M.S., Brockway, K.S., Byrnes, E.J., Chen, L., Chen, L., Chen, T.-M., Chin, M.C., Chong, J., Crook, B.E., Czaplinska, A., Dang, C.N., Datta, S., Dee, N.R., Desaki, A.L., Desta, T., Diep, E., Dolbeare, T.A., Donelan, M.J., Dong, H.-W., Dougherty, J.G., Duncan, B.J., Ebbert, A.J., Eichele, G., Estin, L.K., Faber, C., Facer, B.A., Fields, R., Fischer, S.R., Fliss, T.P., Frensley, C., Gates, S.N., Glattfelder, K.J., Halverson, K.R., Hart, M.R., Hohmann, J.G., Howell, M.P., Jeung, D.P., Johnson, R.A., Karr, P.T., Kawal, R., Kidney, J.M., Knapik, R.H., Kuan, C.L., Lake, J.H., Laramee, A.R., Larsen, K.D., Lau, C., Lemon, T.A., Liang, A.J., Liu, Y., Luong, L.T., Michaels, J., Morgan, J.J., Morgan, R.J., Mortrud, M.T., Mosqueda, N.F., Ng, L.L., Ng, R., Orta, G.J., Overly, C.C., Pak, T.H., Parry, S.E., Pathak, S.D., Pearson, O.C., Puchalski, R.B., Riley, Z.L., Rockett, H.R., Rowland, S.A., Royall, J.J., Ruiz, M.J., Sarno, N.R., Schaffnit, K., Shapovalova, N.V., Sivisay, T., Slaughterbeck, C.R., Smith, S.C., Smith, K.A., Smith, B.I., Sodt, A.J., Stewart, N.N., Stumpf, K.-R., Sunkin, S.M., Sutram, M., Tam, A., Teemer, C.D., Thaller, C., Thompson, C.L., Varnam, L.R., Visel, A., Whitlock, R.M., Wohnoutka, P.E., Wolkey, C.K., Wong, V.Y., Wood, M., Yaylaoglu, M.B., Young, R.C., Youngstrom, B.L., Yuan,

X.F., Zhang, B., Zwingman, T.A., Jones, A.R., 2007. Genome-wide atlas of gene expression in the adult mouse brain. Nature 445, 168–176. doi:10.1038/nature05453

Liu, C., Kershberg, L., Wang, J., Schneeberger, S., Kaeser, P.S., 2018. Dopamine Secretion Is Mediated by Sparse Active Zone-like Release Sites. Cell 172, 706–718.e15. doi:10.1016/j.cell.2018.01.008

Liu, F., Wan, Q., Pristupa, Z.B., Yu, X.M., Wang, Y.T., Niznik, H.B., 2000. Direct protein-protein coupling enables cross-talk between dopamine D5 and gamma-aminobutyric acid A receptors. Nature 403, 274–280. doi:10.1038/35002014

Luquet, E., Biesemann, C., Munier, A., Herzog, E., 2016. Purification of Synaptosome Populations Using Fluorescence-Activated Synaptosome Sorting, in: Methods in Molecular Biology, Methods in Molecular Biology. Springer New York, New York, NY, pp. 121–134. doi:10.1007/978-1-4939-6688-2_10

Moss, J., Bolam, J.P., 2008. A dopaminergic axon lattice in the striatum and its relationship with cortical and thalamic terminals. J Neurosci 28, 11221–11230. doi:10.1523/JNEUROSCI.2780-08.2008

Oh, S.W., Harris, J.A., Ng, L., Winslow, B., Cain, N., Mihalas, S., Wang, Q., Lau, C., Kuan, L., Henry, A.M., Mortrud, M.T., Ouellette, B., Nguyen, T.N., Sorensen, S.A., Slaughterbeck, C.R., Wakeman, W., Li, Y., Feng, D., Ho, A., Nicholas, E., Hirokawa, K.E., Bohn, P., Joines, K.M., Peng, H., Hawrylycz, M.J., Phillips, J.W., Hohmann, J.G., Wohnoutka, P., Gerfen, C.R., Koch, C., Bernard, A., Dang, C., Jones, A.R., Zeng, H., 2014. A mesoscale connectome of the mouse brain. Nature 508, 207. doi:10.1038/nature13186

Pellissier, F., Gerber, A., Bauer, C., Ballivet, M., Ossipow, V., 2007. The adhesion molecule Necl-3/SynCAM-2 localizes to myelinated axons, binds to oligodendrocytes and promotes cell adhesion. BMC Neurosci 8, 90. doi:10.1186/1471-2202-8-90

Pereira, D.B., Schmitz, Y., Mészáros, J., Merchant, P., Hu, G., Li, S., Henke, A., Lizardi-Ortiz, J.E., Karpowicz, R.J., Morgenstern, T.J., Sonders, M.S., Kanter, E., Rodriguez, P.C., Mosharov, E.V., Sames, D., Sulzer, D., 2016. Fluorescent false neurotransmitter reveals functionally silent dopamine vesicle clusters in the striatum. Nat Neurosci 19, 578–586. doi:10.1038/nn.4252

Poulopoulos, A., Aramuni, G., Meyer, G., Soykan, T., Hoon, M., Papadopoulos, T., Zhang, M., Paarmann, I., Fuchs, C., Harvey, K., Jedlicka, P., Schwarzacher, S.W., Betz, H., Harvey, R.J., Brose, N., Zhang, W., Varoqueaux, F., 2009. Neuroligin 2 drives postsynaptic assembly at perisomatic inhibitory synapses through gephyrin and collybistin. Neuron 63, 628–642. doi:10.1016/j.neuron.2009.08.023

Poulopoulos, A., Murphy, A.J., Ozkan, A., Davis, P., Hatch, J., Kirchner, R., Macklis, J.D., 2019. Subcellular transcriptomes and proteomes of developing axon projections in the cerebral cortex. Nature 1. doi:10.1038/s41586-018-0847-y

Rasband, W.S., 1997. ImageJ, U.S. National Institutes of Health, Bethesda, Maryland, USA. http://rsb.info.nih.gov/ij/.

Sagné, C., Mestikawy, El, S., Isambert, M.F., Hamon, M., Henry, J.P., Giros, B., Gasnier, B., 1997. Cloning of a functional vesicular GABA and glycine transporter by screening of genome databases. FEBS Lett 417, 177–183.

Schreiner, D., Savas, J.N., Herzog, E., Brose, N., de Wit, J., 2016. Synapse biology in the "circuit-age-"paths toward molecular connectomics. Curr Opin Neurobiol 42, 102–110. doi:10.1016/j.conb.2016.12.004

Sesack, S.R., Aoki, C., Pickel, V.M., 1994. Ultrastructural localization of D2 receptor-like immunoreactivity in midbrain dopamine neurons and their striatal targets. J Neurosci 14, 88–106.

Surmeier, D.J., Ding, J., Day, M., Wang, Z., Shen, W., 2007. D1 and D2 dopamine-receptor

modulation of striatal glutamatergic signaling in striatal medium spiny neurons. Trends Neurosci 30, 228–235. doi:10.1016/j.tins.2007.03.008

Tellez, L.A., Han, W., Zhang, X., Ferreira, T.L., Perez, I.O., Shammah-Lagnado, S.J., van den Pol, A.N., de Araujo, I.E., 2016. Separate circuitries encode the hedonic and nutritional values of sugar. Nat Neurosci 19, 465–470. doi:10.1038/nn.4224

Tellez, L.A., Medina, S., Han, W., Ferreira, J.G., Licona-Limón, P., Ren, X., Lam, T.T., Schwartz, G.J., de Araujo, I.E., 2013. A gut lipid messenger links excess dietary fat to dopamine deficiency. Science 341, 800–802. doi:10.1126/science.1239275

Thomas, L.A., Akins, M.R., Biederer, T., 2008. Expression and adhesion profiles of SynCAM molecules indicate distinct neuronal functions. J Comp Neurol 510, 47–67. doi:10.1002/cne.21773

Turiault, M., Parnaudeau, S., Milet, A., Parlato, R., Rouzeau, J.-D., Lazar, M., Tronche, F., 2007. Analysis of dopamine transporter gene expression pattern -- generation of DAT-iCre transgenic mice. FEBS J. 274, 3568–3577. doi:10.1111/j.1742-4658.2007.05886.x

Uchigashima, M., Ohtsuka, T., Kobayashi, K., Watanabe, M., 2016. Dopamine synapse is a neuroligin-2-mediated contact between dopaminergic presynaptic and GABAergic postsynaptic structures. Proc Natl Acad Sci USA 113, 4206–4211. doi:10.1073/pnas.1514074113

Van der Krogt, J.A., Koot-Gronsveld, E., Van den Berg, C.J., 1983. Subcellular fractionation of striatum: sedimentation properties of dopaminergic synaptosomes. Life Sci. 33, 605–613.

Varoqueaux, F., Jamain, S., Brose, N., 2004. Neuroligin 2 is exclusively localized to inhibitory synapses. Eur. J. Cell Biol. 83, 449–456. doi:10.1078/0171-9335-00410

Whittaker, V.P., 1993. Thirty years of synaptosome research. J. Neurocytol. 22, 735–742.

Yagishita, S., Hayashi-Takagi, A., Ellis-Davies, G.C.R., Urakubo, H., Ishii, S., Kasai, H., 2014. A critical time window for dopamine actions on the structural plasticity of dendritic spines. Science 345, 1616–1620. doi:10.1126/science.1255514

Yan, X., Wang, Z., Schmidt, V., Gauert, A., Willnow, T.E., Heinig, M., Poy, M.N., 2018. Cadm2 regulates body weight and energy homeostasis in mice. Mol Metab 8, 180–188. doi:10.1016/j.molmet.2017.11.010

Zhu, F., Cizeron, M., Qiu, Z., Benavides-Piccione, R., Kopanitsa, M.V., Skene, N.G., Koniaris, B., DeFelipe, J., Fransén, E., Komiyama, N.H., Grant, S.G.N., 2018. Architecture of the Mouse Brain Synaptome. Neuron 99, 781–799.e10. doi:10.1016/j.neuron.2018.07.007

METHODS

Animals

A transgenic mouse line expressing *cre* recombinase under the control of the dopamine transporter (DAT) was used (Turiault et al., 2007). Mice were maintained in C57BL/6N background and housed in 12/12 LD with ad libitum feeding. Every effort was made to minimize the number of animals used and their suffering. The experimental design and all procedures were in accordance with the European guide for the care and use of

laboratory animals and approved by the ethics committee of Bordeaux University (CE50) and the French Ministry of Research under the APAFIS n° 8944.

AAV Vector and stereotaxic injection

Stereotaxic injections were performed in heterozygous DAT-*cre*$^+$ and wild-type (WT) mice of either sex at 8 to 9 weeks of age(as described in Cetin et al., 2006). An Adeno-Associated Virus (AAV) containing an inverted sequence of EGFP-coding gene flanked by loxP-sites (AAV1 pCAG-FLEX-EGFP-WPRE, University of Pensylvania)(Oh et al., 2014) was injected into DAT-*cre*$^+$ mice (Figure 1 Panel 1). Saline injected littermates were used as auto-fluorescence controls. The stereotaxic injections were performed in Isoflurane-anesthetized mice using a 30µl glass micropipette. Injection coordinates for the Substantia Nigra pars compacta (SNc) were anterior/posterior (A/P) - 3.6 mm, lateral (L) +/- 1.3mm, dorsal/ventral (D/V) - 4.2mm. Injection coordinates for the Ventral Tegmental (VTA) were A/P - 3.6mm , L +/- 0.6mm; D/V - 3.9mm. A/P and L coordinates are given with respect to the *bregma*, whereas D/V coordinates are given with respect to the brain surface (Figure 1 Panel 1). The animals were euthanized after 28 days at the maximal viral EGFP expression. For fluorescence activated synaptosome sorting (FASS) experiments, four to six DAT-*cre*$^+$ mice and one WT mouse were used.

Subcellular fractionation of synaptosomes

The preparation of sucrose synaptosomes was adapted from a previously published protocol (De-Smedt-Peyrusse et al., 2018). Animals were euthanized by cervical dislocation, decapitated and the head was immersed in liquid nitrogen for a few seconds. Bright fluorescent parts of the striatum of WT and DAT-*cre*$^+$ mice were subsequently dissected under an epi-fluorescence stereomicroscope (Leica Microsystems, Germany, Figure 1 Panel 2). Non-fluorescent control striata were dissected following anatomical borders. Samples were then homogenized in 1ml of ice-cold Isosmolar buffer (0.32M sucrose, 4mM HEPES pH7.4, protease inhibitor cocktail Set 3 EDTA-free (EMD Millipore Corp.)) using a 2ml-glass-Teflon homogenizer with 12 strokes at 900 rpm. The homogenizer was rinsed with 250µL of isosmolar buffer and 3 manual strokes and then, the pestle was rinsed with additional 250µl of isosmolar buffer. The final 1.5ml of homogenate (H) was centrifuged at 1000xg for 5min at 4°C in a benchtop microcentrifuge. The supernatant (S1) was separated from the pellet (P1) and centrifuged at 12,600xg for 8min at 4°C. The supernatant (S2) was discarded and the synaptosomes-enriched pellet (P2) was resuspended in 1ml of isosmolar buffer and layered on a two-step sucrose density gradient (900µl of 1.2M and 900µl of 0.8M sucrose, 4mM HEPES). The gradient was centrifuged at 50,000xg for 21min at 4°C

(Beckman Coulter Optima MAX XP ultracentrifuge with a TL-55 rotor). Sucrose synaptosomes were recovered at the 0.8 and 1.2 M sucrose interface using a 0.5ml syringe.

Fluorescence Activated Synaptosome Sorting (FASS) workflow

After collection, sucrose synaptosomes were stored on ice and sequentially diluted in ice-cold PBS with protease inhibitor as described above, and the lipophilic dye FM4-64 dye was added at 1µg/ml to the solution to red label all membrane particles (Figure 1A). The FACSAria-II (BD Biosciences) was operated with the following settings: 70µm Nozzle, sample shaking 300rpm at 4°C, FSC neutral density (ND) filter 1.0, 488nm laser on, area scaling 1.18, window extension 0.5, sort precision 0-16-0, FSC (340 V), SSC (488/10nm, 365V), FITC (EGFP) (530/30nm, 700V), PerCP (FM4-64) (675/20 nm, 700 V). Thresholding on FM4-64 was set with a detection threshold at 800. Samples were analyzed and sorted at rates of 15,000-20,000 events/s and flow rate of 3. Unsorted synaptosomes ("singlet" gate) and FASS synaptosomes ("EGFP+" sub-gate of the "singlet" gate) were collected sequentially (Figures 1 and S1). After sorting, samples were either centrifuged on gelatinized coverslips of 12mm diameter ($5x10^5$ synaptosomes per coverslip at 6,800xg for 34min at 4°C Beckman J-26XP with a JS 5.3 rotor), or filtered on 0.1µm Isopore polycarbonate filters (Merck-Milipore). Coverslips were then further treated and analyzed either for immunofluorescence imaging or for electron microscopy while filtered samples underwent mass spectrometry analysis (Figure 1A).

Immunofluorescence

Synaptosomes on coverslips were fixed (4% paraformaldehyde, 4% sucrose, PBS) for 10min at room temperature, washed three times with PBS for 5min and then stored at 4°C until use. Synapstosomes were blocked and permeabilized with PGT buffer (PBS, 2g/L gelatin, 0.25% Triton X-100) and subsequently incubated with primary antibodies in PGT buffer (1h at room temperature), washed 3 times with PGT and incubated with secondary antibodies in PGT (1 hour at room temperature). Three final washes with PGT buffer were performed prior to a washing step in PBS and a final rinse in ultrapure water. Coverslips were mounted on glass slides with Fluoromount-G mounting solution (Sigma) and stored at 4°C until observation.

Antibodies

The following primary antibodies were used. Anti-SynCAM2, rat antibody (provided by Thomas Biederer). anti-D1 receptor, goat polyclonal antibody (Frontier Institute Cat# D1R-Go-Af1000, RRID: AB_2571594). Guinea pig polyclonal antibody to: VGLUT2 (Millipore Cat# AB2251, RRID:AB_1587626); VGLUT1 (Millipore Cat# AB5905,

RRID:AB_2301751). Mouse monoclonal antibody to: GFP (Roche Cat# 11814460001, RRID:AB_390913); Gephyrin (Synaptic Systems Cat# 147 111, RRID: AB_887719). Rabbit polyclonal antibodies to: Tyrosine Hydroxylase (Synaptic Systems Cat# 213 102, RRID:AB_2619896); D2 dopamine receptor (Millipore Cat# ABN462, RRID:AB_2094980); Synapsin 1/2 (Synaptic Systems Cat# 106 002, RRID:AB_887804); VGLUT2 (Cat# VGLUT2, RRID:AB_2315563) (Herzog et al., 2001); VIAAT/VGATs (Synaptic Systems Cat# 131 002, RRID:AB_887871); DAT (Millipore Cat# AB2231, RRID: AB 1586991); EAAT1/GLAST (Cat# Ab#314, RRID:AB_2314561 a kind gift by Niels Christian Danbolt, university of Oslo)(Holmseth et al., 2009).

Proteomics

10^7 EGFP+ singlets synaptosomes were accumulated for proteomics analysis and were compared to 10^6 all singlets particles (unsorted). Both samples were treated in parallel at all steps. Protein samples were solubilized in Laemmlli buffer and underwent a short separation using SDS-PAGE. After colloidal blue staining, whole lanes were cut in 1 cm x 1 cm gel pieces. Gel slices were destained in 25 mM ammonium bicarbonate 50% acetonitrile (ACN), shrunk in ACN for 10 min. After ACN removal, gel pieces were dried at room temperature, covered with trypsin solution (10 ng/µl in 40 mM NH_4HCO_3 and 10% ACN), rehydrated at 4 °C for 10 min and incubated overnight at 37 °C. Spots were then incubated for 15 min in 40 mM NH_4HCO_3 and 10% ACN at room temperature with rotary shaking. The supernatant was collected and an H_2O/ACN/HCOOH (47.5:47.5:5) extraction solution was added onto gel pieces for 15 min. The extraction step was repeated twice. Supernatants were pooled and concentrated in a vacuum centrifuge before being resuspended in 30 µl 0.1% formic acid.

Peptide mixture was analyzed on a Ultimate 3000 nanoLC system (Dionex, Amsterdam, The Netherlands) coupled to a Electrospray Q-Exactive quadrupole Orbitrap benchtop mass spectrometer (Thermo Fisher Scientific, San Jose, CA). 10 µl of peptide digests were loaded onto a 300-µm-inner diameter x 5-mm C_{18} PepMap™ trap column (LC Packings) at a flow rate of 30 µl/min. The peptides were eluted from the trap column onto an analytical 75-mm id x 25-cm C18 Pep-Map column (LC Packings) with a 4–40% linear gradient of solvent B in 108 min (solvent A was 0.1% formic acid in 5% ACN, and solvent B was 0.1% formic acid in 80% ACN). Separation flow rate was 300 nl/min and the mass spectrometer operated in positive ion mode at a 1.8-kV needle voltage. Data were acquired using Xcalibur 2.2 software in a data-dependent mode. MS scans (*m/z* 300-2000) were recorded at a resolution of R = 70000 (@ m/z 200) and an AGC target of 10^6 ions collected within 100 ms. Dynamic exclusion was set to 30 s and top 15 ions were selected from fragmentation in HCD mode.

MS/MS scans with a target value of 1 x 10^5 ions were collected with a maximum fill time of 120 ms and a resolution of R = 35000. Additionally, only +2 and +3 charged ions were selected for fragmentation. Other settings were as follows: no sheath nor auxiliary gas flow, heated capillary temperature, 250 °C; normalized HCD collision energy of 25% and an isolation width of 3 m/z.

Data were searched by SEQUEST through Proteome Discoverer 1.4 (Thermo Fisher Scientific Inc.) against *Mus musculus* reference Proteome Set (Uniprot 2017-05; 50885 entries). Spectra from peptides higher than 5000 Da or lower than 350 Da were rejected. The search parameters were as follows: mass accuracy of the monoisotopic peptide precursor and peptide fragments was set to 10 ppm and 0.02 Da respectively. Only b- and y-ions were considered for mass calculation. Oxidation of methionines (+16 Da) and carbamidomethylation (+57 Da) and propionamidation of cysteines (+71 Da) were considered as variable modification. Two missed trypsin cleavages were allowed. Peptide validation was performed using Percolator algorithm[46] and only "high confidence" peptides were retained corresponding to a 1% False Positive Rate at peptide level.

Epifluorescence Microscopy and Image processing

Immuno-stained synaptosomes were imaged using either a Nikon Eclipse NiU (with a 40x/NA 0.75 dry objective equipped with a sCMOS ANDOR Zyla 5.5 sCMOS camera) or a Leica DMI8 epifluorescence microscope (with a 63x/NA 1.4 oil immersion objective equipped with a sCMOS Hamamatsu FLASH 4.0v2 camera; Figure 1). Adequate imaging parameters were determined prior to each acquisition. About ten to twenty areas were chosen randomly on each coverslip and imaged using neutral density filters to prevent bleaching.

Correlation of synaptosomes' labelling has been automated by generating a home-made macro-command, using the ImageJ software (Rasband, 1997) (18.02.19.Quantification.de.colocalisation.sur.synaptosomes.Herzog.Etienne.v5.ijm). The workflow is composed of three steps. First, the images are pre-processed. The original images, transtyped to 32-bits, are centered and reduced: their respective average intensity is subtracted and division by their standard deviation is performed. It is assumed that both signals lay close one from the other: both images are therefore combined into one to serve for synaptosomes' detection. On each pixel, the maximum signal from both channels is retained to produce a new image, which will be subjected to both median filtering and gaussian blurring (3 pixels radius). Each potential synaptosome now appears as a bell-shaped blob, which center might be determined using a local maximum detection (tolerance to noise: 3). Second, the detections are reviewed and user-validated. Part of the original images is cropped around the local

maxima and displayed to the user as a mosaic. Each thumbnail is displayed on a clickable frame, allowing the user to include or reject a synaptosome from analysis. Criteria of rejection included: presence of competing particles in the quantification area, bad focus on the particle, proximity of the image border preventing proper quantification. Finally, data is extracted, exported and displayed. A circular region is positioned over the center of the thumbnail. The centroid's coordinates are retrieved and logged. From the two sets of coordinates (one per channel) the inter-signal distance is computed. Signal quantification is performed by placing a round region of interest (24 pixels radius) around the centroid, and measuring the integrated intensity. A measurement of the local background is performed, placing a band around the previous region. All values are logged for both channels, for all retained structures and reported in a .CSV file. Further analysis was performed using the FlowJo and GraphPad PRISM softwares. xy-plots of integrated intensity values are displayed with a quadrant analysis of single or double signal detections. Quadrant gates positions were defined from raw images by the experimenter. For all analyses, randomly chosen particles were displayed in a gallery to give an overview of the population analyzed (Figure 1C).

To assess the distance between two labeled dots, a plugin for ImageJ was developed. First, a binary representation of both original images was generated by a wavelet filtering algorithm (J. E. Fowler, n.d.), allowing identification of the immuno-labels as individual objects. Each object was then represented by their barycenter. Two separated particles were considered associated if $d < 2$ µm, with d the Euclidian distance between their barycenter. To statistically determine if these associations were significant or happening by chance, we performed randomization tests. For each color channel, we fixed the position of its particle while randomizing the ones of the other channel. Since there is no underlying structure, the probability of having a particle at a certain position is identical for the whole image space. Consequently, randomization was performed by generating a complete spatial random distribution having the same number of points as the number of particles of the channel being randomized. Associations between 2 markers were then computed as explained above. The final random association values reported were defined as the mean of 10,000 randomizations.

STimulated Emission Depletion (STED) Microscopy

Images were acquired using a Leica TCS SP8/STED3X microscope equipped with a HC PL APO 93X/1.30 GLYC motCORR – STED WHITE objective. We used depletion laser lines at 592nm for Alexa488 and 775nm for Alexa594 or ATTO647n fluorophores. A 25% 3D-STED effect was applied to increase Z resolution. Metrology measurements were

regularly performed using fluorescent beads to test proper laser alignment. Less than 2 pixels shift between channels was measured.

Electron Microscopy

Synaptosomes for transmission electron microscopy (Figure 1D) were fixed right after centrifugation on coverslips with a 1% Glutaraldehyde and 2% PFA (Electron Microscopy Sciences) in PBS solution and kept at 4°C until further treatment. They were then washed with PB and post-fixed in 1% osmium tetroxide and 1% K3Fe(CN)6 in PB, for 2h on ice in the dark. Washed in H_2O and dehydrated in an ascending series of ethanol dilutions (10min in 50% ethanol, 10min in 70% ethanol, twice 15min in 95% ethanol, twice 20 min in absolute ethanol). After absolute ethanol, coverlips were lifted into Epon 812 resin (Electron Microscopy Sciences) and 50% ethanol for 2h at room temperature and then left in pure resin overnight at 4°C. Coverslips were then placed on microscope slides, embedded with capsules filled by pure resin and polymerised at 60°C for 48h. The resin block was then trimmed with razor blades. Sections, 65nm thick, were then cut using a diamond knife Ultra 35° (Diatome) with an ultra-microtome (Leica UC7) and collected on 150 mesh copper grids (Electron Microscopy Sciences).

The sections were stained with UranyLess® (Chromalys and Deltamicroscopy) Sample were then observed with an Hitachi H7650 transmission electron microscope equipped with a Gatan Orius CCD camera. Synaptosomes were identified by their size (0.5 - 2µm), their shape and the presence of intracellular compartments and organelles such as vesicles.

FIGURE LEGENDS

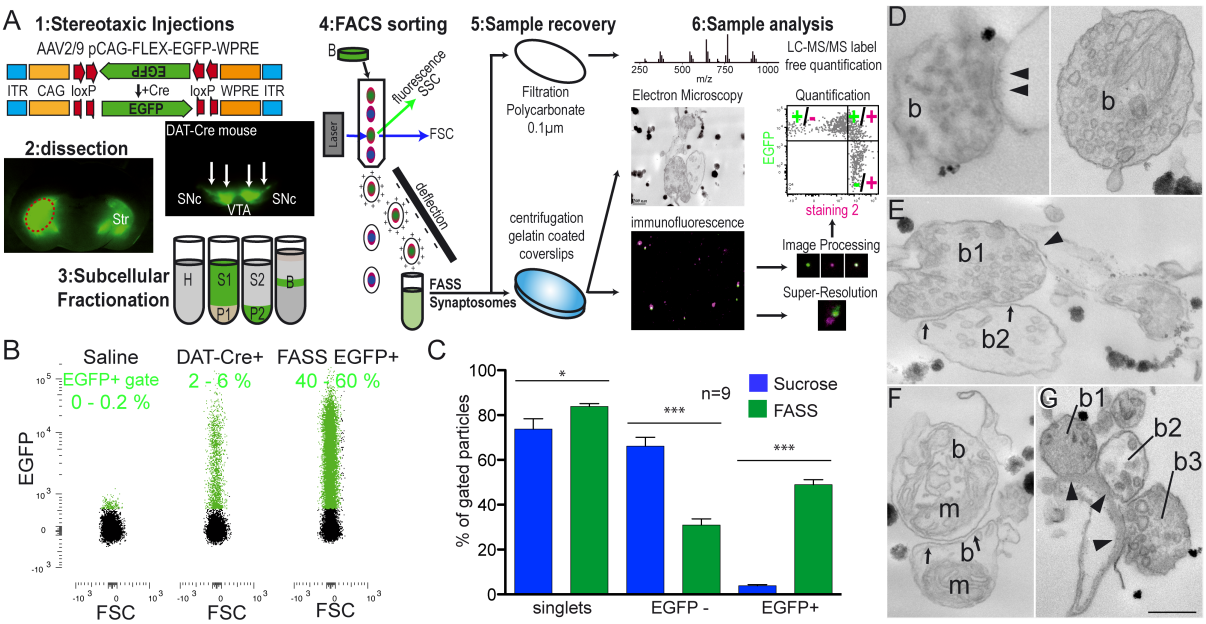

Figure 1: single projection Fluorescence Activated Synaptosome Sorting (FASS) isolates dopaminergic hub synaptosomes (A) Workflow of DAT-cre/AAV-EGFP based synaptosome sorting and analysis. (1) DAT-Cre+ mice stereotaxically injected with a Cre-dependent AAV expressing EGFP in the Substantia Nigra pars compacta and the Ventral Tegmental Area. (2) Dissection of brightest fluorescent part of Striatum (Str) (red-dashed circle). (3) Synaptosome subcellular fractionation on a discontinuous sucrose gradient and (4) FASS. (5) Collection by filtration or centrifugation on glass coverslips. (6) FASS sample analysis by mass spectrometry, electron microscopy, conventional and super-resolved immunofluorescence. **(B)** Analysis of synaptosomes through FASS sorting. (left) Saline synaptosomes determine the level of autofluorescence. Gating was set to have 0-0.2% of particles within the EGFP+ range in negative controls. (middle) Sucrose DAT-Cre+ synaptosome before sorting show 2-6% of EGFP+ particles. (right) FASS EGFP+ synaptosomes reanalysed in the sorter consist of 40-60% of EGFP+ particles. See Figure S1 for detailed gating strategy **(C)** Average DAT-cre+/EGFP FASS results. Sucrose (blue) and FASS (green) samples for the different gates: singlets, EGFP-, EGFP+. Note the steep increase in EGFP+ particles and significant decrease in EGFP- contaminants through the FASS process. n=9 sorts, all data are mean ±SEM. ***$p < 0.001$, *$p < 0.05$. paired t-tests. **(D-**

G) Electron micrographs of sorted synaptosomes. **(D)** Typical synaptosomes displaying synaptic vesicles (SV) rich bouton (b, left and right) and synaptic contact (arrowhead) with an opened postsynaptic membrane (left only). **(E)** Example of synaptic hub displaying a SV-rich bouton (b1, upper) contacting a postsynaptic membrane (arrowheads) and a second bouton (arrows) less populated with SVs (b2, lower). **(F)** example of a synaptic hub structure cut through a plan that is not optimal to identify all synaptic elements. **(G)** Synaptic hub displaying 3 distinct presynaptic profiles (b1, b2, and b3) contacting a postsynaptic membrane (arrowheads). Note the middle bouton (b2) less populated with SVs. Scale bar, 200 nm. Unspecific electron dense precipitates result from the embedding of synaptosomes on gelatin chrome-alum coating.

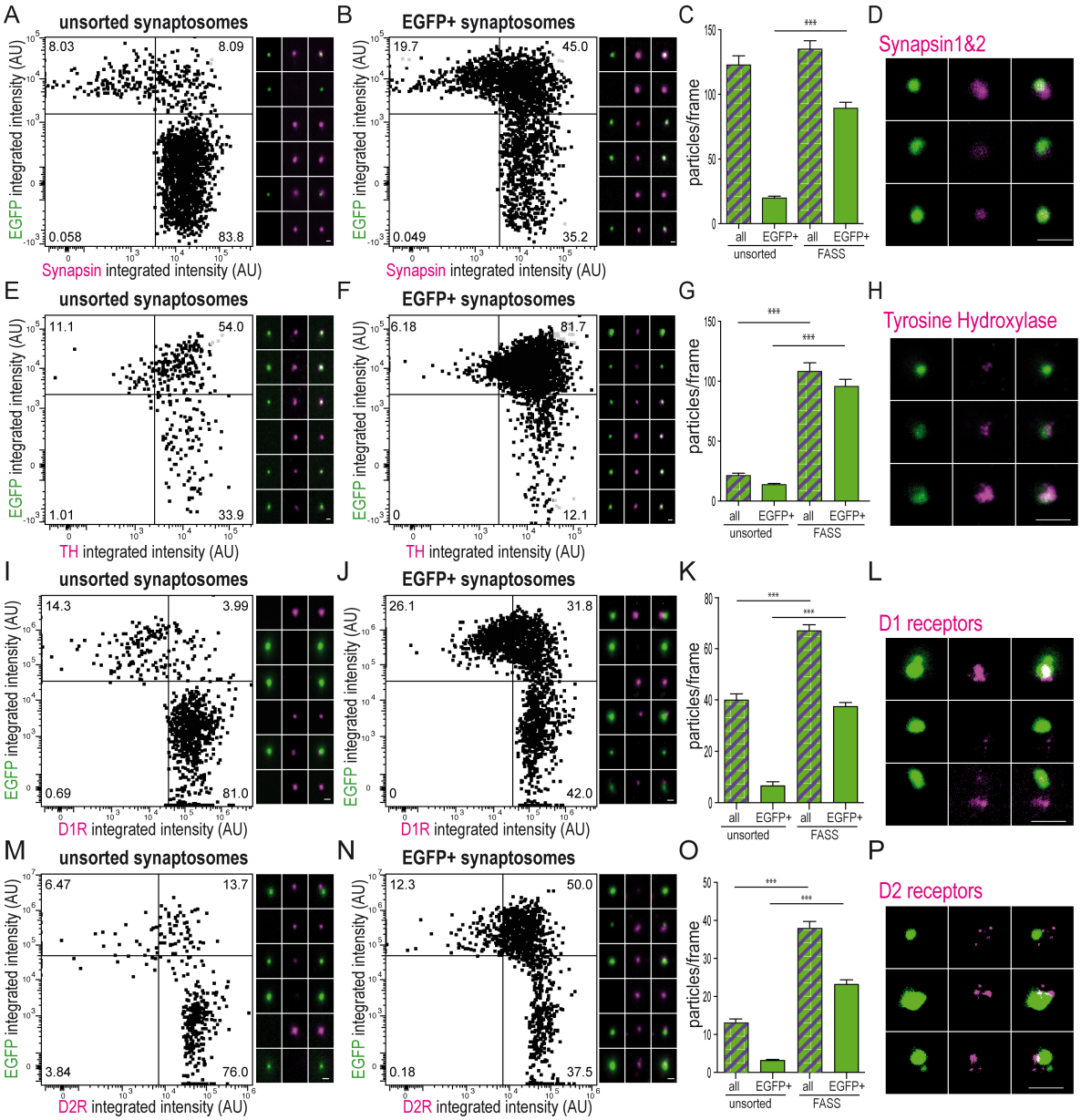

Figure 2: Immunofluorescence analysis of FASS synaptosomes reveal the enrichment for pre- and post-synaptic dopaminergic markers (A-B) Dot plots of anti-Synapsin1&2 (x-axis) and anti-EGFP (y-axis) intensity signals of unsorted and EGFP+ FASS synaptosomes (left). Representative epifluorescence images of analyzed particles. Note that synapsin signals are colocalised with EGFP but also closely apposed. EGFP+/Synapsin+ particles increases from 8.09% in unsorted to 45% in EGFP+ synaptosomes samples (upper right quadrant). **(C)** Quantification of (A) and (B) showing the total versus EGFP+ number of immuno-detected particles per frame. EGFP+ particle numbers increases significantly in the FASS sample

while the total number of labeled particles is relatively stable. n = 3 sorts, mean ±SEM, ***p < 0.001, **p < 0.01. paired t-test. **(D)** Representative stimulated emission depletion (STED) microscopy images of synaptosomes stained for EGFP (green) and Synapsin1&2 (magenta). **(E-F)** Same as A-B for EGFP and Tyrosine Hydroxylase. Double positive particles population increases from 54% (E) to 81.7% (F). **(G)** same as C showing numbers of particles per frame. Immuno-detections increase by 5-fold in the FASS sample compared to unsorted. n=3 sorts, mean ±SEM, ***p < 0.001. paired t-test. **(H)** STED images of EGFP (green) and TH (magenta) labeled synaptosomes. Note the nearly perfect colocalizations. **(I-J)** Same as A-B for EGFP and D1 dopamine receptors. Double labeled populations increase from 3.99% (I) to 31.8% (J). Note that D1R positives represent about 55% of EGFP+ (dopaminergic) particles, while D1R+/EGFP- may represent extrasynaptic receptors on contaminants of the FASS sample. **(K)** Number of particles immuno-detected per frame. n=3, mean ±SEM, ***p < 0.001. paired t-test. **(L)** STED microscopy detects D1 receptor clusters (magenta) aposed to the EGFP+ synaptosomes (green). **(M-N)** Same as A-B for anti-EGFP and anti-D2 dopamine receptors. Double positive synaptosome representation increases from 13.7% (M) to 50% (N). **(K)** Number of particles immuno-detected per frame. n=3 sorts, mean ±SEM, ***p < 0.001. paired t-test. **(L)** STED images display D2R (magenta) patches apposed to EGFP (green). For all panels, scale bar = 1 μm. See extra immunofluorescence analysis in Figure S2.

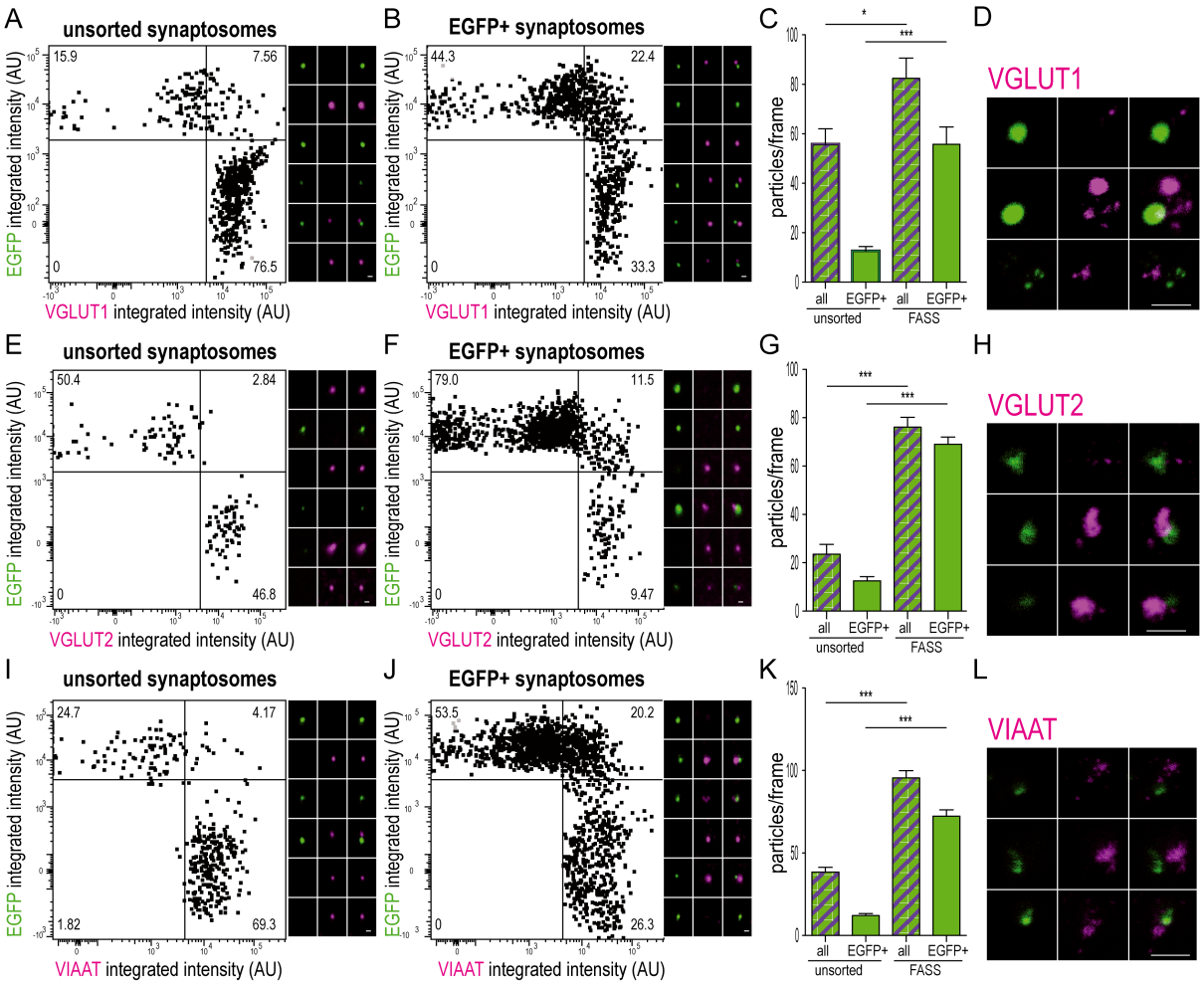

Figure 3: Dopaminergic varicotisties associate with glutamatergic and GABAergic synapses in "hub synapses". (A-B) Dot plots of anti-VGLUT1 (x-axis) and anti-EGFP (y-axis) intensity signals of unsorted and EGFP+ FASS synaptosomes (left). Representative epifluorescence images of analyzed particles. Images display a frequent aposition of VGLUT1+ dots and EGFP+ dots. Note the unexpected enrichment of EGFP+/VGLUT1+ synaptosomes from 7.5% to 22.4% upon sorting (upper right quadrant). Instead, EGFP-/VGLUT1+ synaptosomes are 2-fold reduced as expected during sorting (lower right quadrant). **(C)** Quantification of (A) and (B) showing the total versus EGFP+ number of immuno-detected particles per frame. EGFP+ particle numbers increases significantly in the FASS sample. n=3 sorts, mean ±SEM, ***p < 0.001, *p < 0.1. paired t-test. **(D)** Representative STED images of synaptosomes stained for EGFP (green) and VGLUT1 (magenta). VGLUT1 puncta are distantly apposed to EGFP puncta. **(E-F)** Same as A-B for

EGFP and VGLUT2 labeling mainly thalamo-striatal terminals. The EGFP+/VGLUT2+ population increases from 2.84% (E, upper-right quadrant) to 11.5% (F, upper-right quadrant). **(G)** Same as C showing numbers of particles per frame. n=3, mean±SEM, ***p<0.001. paired t-test. **(H)** STED images display VGLUT2 puncta (magenta) apposed to EGFP puncta (green). **(I-J)** Same as A-B for EGFP and inhibitory terminals labeled by VIAAT, the vesicular inhibitory amino-acid transporter. EGFP+/VIAAT+ particles representation increases from 4.17% (I, upper-right quadrant) to 20.2% (J, upper-right quadrant). **(K)** Same as C showing numbers of particles per frame. n=3, mean±SEM, ***p<0.001. paired t-test. **(L)** STED images display apposition of EGFP (green) and VIAAT (magenta) signals. Scale bars, 1 µm. See Figures S3-S4 and table 1 for negative and positive controls to "hub synapse" associations.

Imunolabelings	Observed associations (%)	simulated associations (%)
EGFP + VGLUT1	22.4	0.94
EGFP + VGLUT2	11.5	0.23
EGFP + VIAAT	20.2	0.67
VGLUT1 + VGLUT2	5.45	1.98
VGLUT1 + TH	37.9	1.40

Table 1: Observed versus simulated randomized associations of immunolabeled markers.

		Unsorted		EGFP+ Sorted	
Gene Name	Description	N peptides	Score	N peptides	Score
Cadm2	**Cell adhesion molecule 2 - SynCAM2**	**/**	**/**	**4**	**5.99**
Slc6a3	**Na^+-dependent dopamine transporter - DAT**	**/**	**/**	**5**	**5.37**
Snap25	Synaptosomal-associated protein 25	6	14.84	8	16.80
Ncam1	Neural cell adhesion molecule 1	7	4.99	5	6.68
Syp	Synaptophysin	2	7.71	2	8.55
Slc17a7	Vesicular glutamate transporter 1 - VGLUT1	2	3.76	2	1.67
Stxbp1	Syntaxin-binding protein 1 – MUNC18-1	2	2.47	1	1.79

Table 2: Identification of SynCAM2 enrichment at dopamine synaptosomes through mass spectrometry.

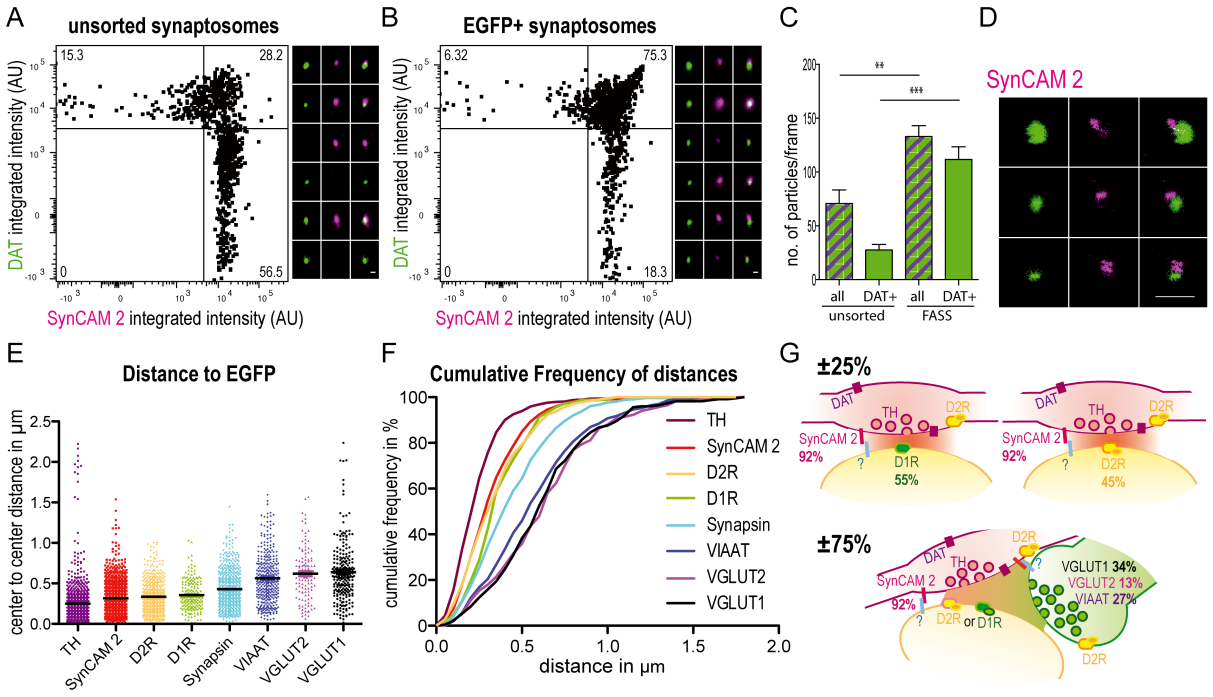

Figure 4: (A-B) Dot plots of anti-SynCAM 2 (x-axis) and anti-DAT (y-axis) intensity signals of unsorted and DAT-EGFP+ FASS synaptosomes (left). Representative epifluorescence images display a frequent tight aposition of SynCAM 2 and DAT. Note the strong enrichment of DAT+/SynCAM 2+ synaptosomes from 28.2% to 75.3% upon sorting (upper right quadrant). Instead, DAT-/SynCAM 2+ synaptosomes are 3-fold reduced as expected during sorting (lower right quadrant). **(C)** Quantification of (A) and (B) showing the number of particles per frame. n=3 sorts, mean ±SEM. ***$p < 0.001$, **$p < 0.01$. paired t-test. **(D)** STED images of synaptosomes stained for DAT (green) and SynCAM 2 (magenta). Scale bars 1 µm. **(E)** Distance to EGFP signal center of all stained proteins in increasing order of average distance. **(F)** Cumulative frequency distribution of distances to EGFP (percentage of all stained molecules). Note the proximity of SynCAM 2 to EGFP and the larger gap left by VGLUT and VIAAT varicosities. **(G)** Model of cellular and molecular architecture of dopamine synapses. Dopamine secretion sites labeled by the DAT-cre strategy are apposed to a postsynaptic element with either D1R (55%) or D2R (45%). In 92% of the cases SynCAM 2 seems to be involved in the synaptic architecture. Though SynCAM1 is a strong candidate,

the counterpart of SynCAM 2 on the postsynaptic membrane remains unknown. Roughly, 75% of dopamine varicosities additionaly forms a synaptic hub with an effector synaptic terminal: VGLUT1+ in 34%, VGLUT2+ in 13% and VIAAT+ in 27% of the cases.

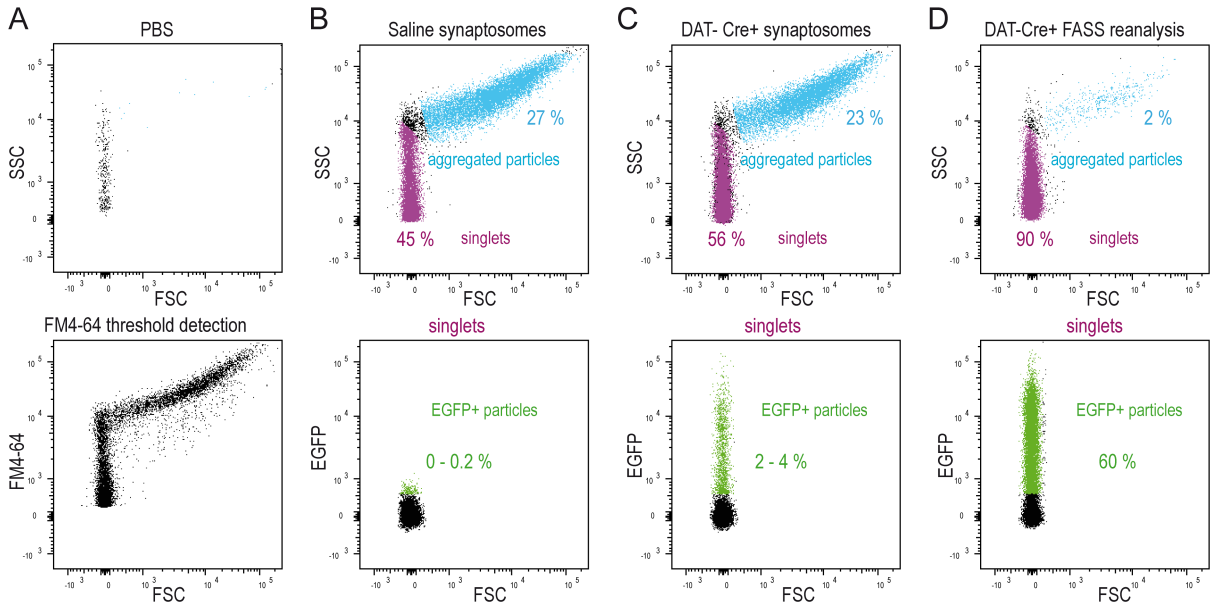

Figure S1: DAT-cre x EGFP FASS gating strategy. (A-D) Representative FASS gate settings and particles detection for EGFP+ DAT-Cre+-synaptosomes sorting. **(A)** Analysis of a PBS sample was used to define background noise in FM4-64 lipopholic styryl dye used for thresholding (top). The noise was less than 500 events per minute. Synaptosome sample detection using FM4-64 thresholding (bottom). Sample dilution was adjusted to reach 20 000 events per second. **(B)** Side scatter (SSC) and forward scatter (FSC) analysis of synaptosomes alows defining aggregated particles (27%, light blue gate) and singlets (45%, magenta gate; top). Singlets gate was defined experimentaly through trials and error as published previously (Luquet et al., 2016). Singlets are further analyzed for EGFP fluorescence (bottom). Saline synaptosomes display low autofluorescence. **(C)** DAT-Cre+ synaptosomes samples showed 23% of aggregated particles and 56% of singlets on this example (top). 2-4% of the singlets were significantly fluorescent in the EGFP channel. **(D)** Particles gated as “singlets” and “EGFP+” were sorted and reanalyzed showing a drop in the proportion of aggregated

particles (2%) and a steep rise in singlets (90%; top). Up to 60% of singlets were EGFP+ (bottom).

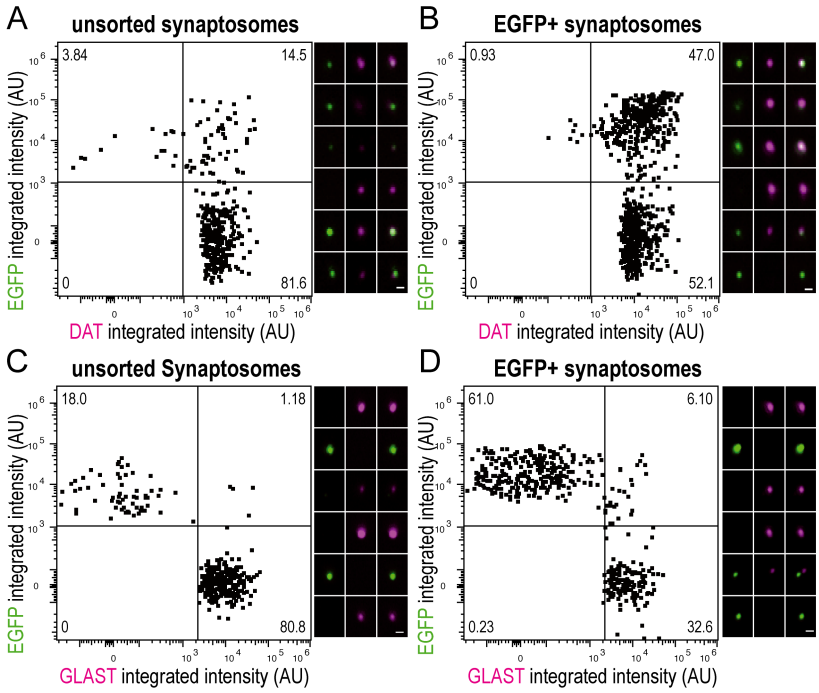

Figure S2: (A-B) Dot plots of unsorted and EGFP+ synaptosomes stained for the dopamine transporter DAT (x-axis) and EGFP (y-axis). Galleries of representative epifluorescence images of individual synaptosomes. Population of particles positive for both EGFP and DAT (upper right quadrant) increases from 14.5% in unsorted to 47% in EGFP+ synaptosomes samples. **(C-D)** Dot plots of intensity signal of unsorted and EGFP+ synaptosomes stained for EGFP and the astrocyte membrane marker EAAT1GLAST and galleries of representative confocal images of analyzed particles. Note the very low representation of double positive particles. Scale bar, 1 μm.

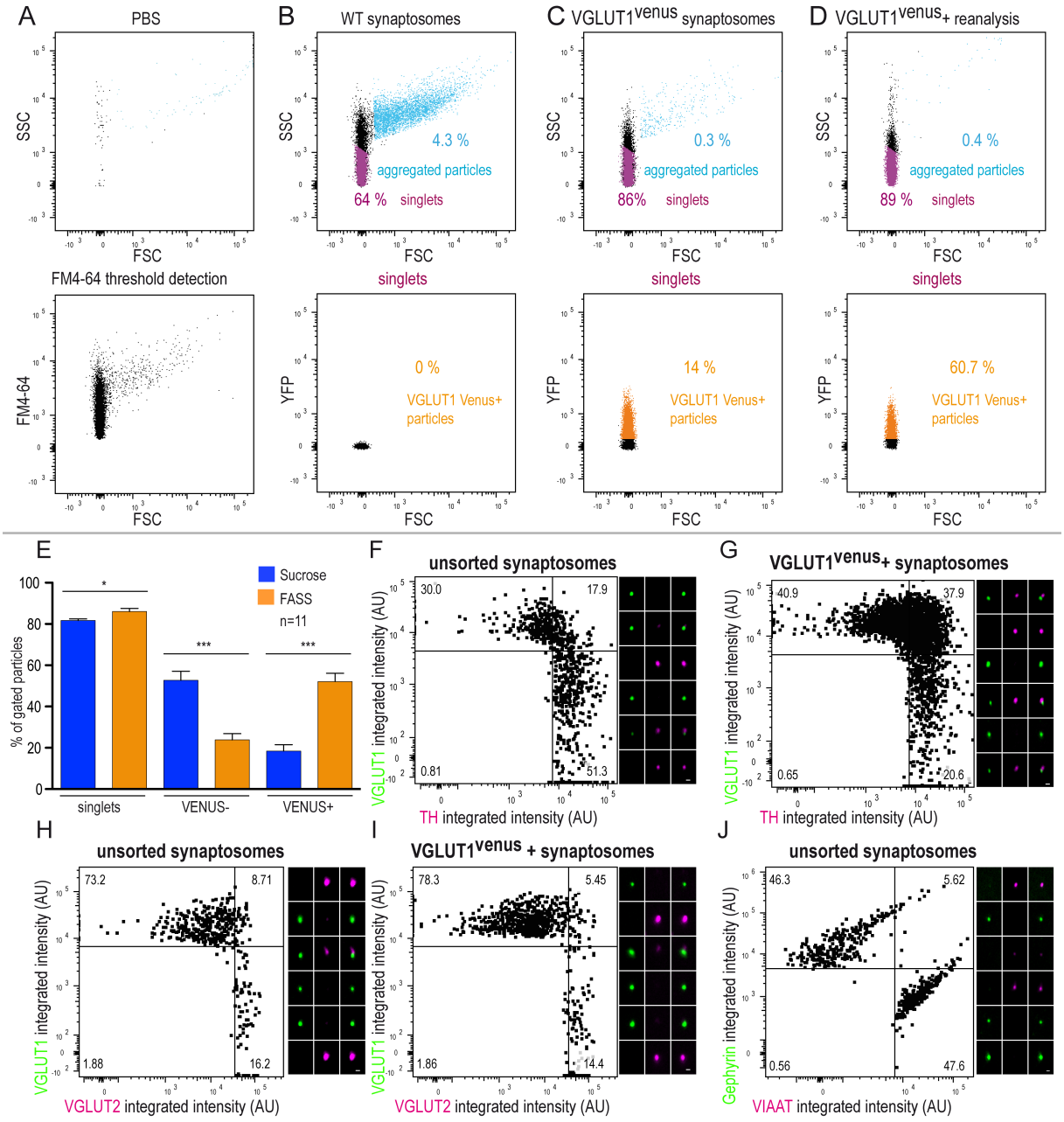

Figure S3: Positive and negative controls to dopamine hub synapse identification. (A-D) Gating strategy for striatal VGLUT1^{venus} FASS. **(A)** Analysis of a PBS sample was used to define background noise in FM4-64 lipopholic styryl dye used for thresholding (top). The noise was less than 500 events per minute. Synaptosome sample detection using FM4-64 thresholding (bottom). Sample dilution was adjusted to reach 20 000 events per second. **(B)** WT synaptosomes display aggregated particles (4.3%, light blue) and singlets (64%, magenta). Singlets gate was defined experimentaly through trials and error as published previously (Luquet et al., 2016). Singlets were further analyzed for Venus fluorescence to determine the

autofluorescence level. **(C)** sucrose VGLUT1^{venus} synaptosomes samples showed 0.3% of aggregated particles and 86% of singlets. 14% of synaptosomes were detected in the venus gate. **(D)** Sorted VGLUT1^{venus} "singlets" were reanalyzed. VGLUT1^{venus} + synaptosomes displayed 0.4% of aggregated particles and 89% singlets. Up to 60.7% of sorted singlets were indeed detected in the venus gate. **(E)** Average striatal VGLUT1^{venus} FASS results. Sucrose (blue) and FASS (orange) samples for the different gates: singlets, VENUS-, VENUS+. Note the steep increase in VENUS+ particles and significant decrease in VENUS- contaminants through the FASS process. n=11 different sorts/condition, all data are mean ±SEM. ***$p < 0.001$, *$p < 0.1$. paired t-test. **(F-G)** Dot plots of unsorted and VGLUT1+ synaptosomes stained for VGLUT1 (y-axis) and TH (x-axis). Galleries of representative epifluorescence images of analyzed particles. VGLUT1^{venus} +/TH+ particles (upper right quadrant) increases from 17.9% in unsorted (F) to 37.9% in VGLUT1^{venus} + sorted synaptosomes (G). A similar situation as for DAT-EGFP synaptosomes (see Figure 3). **(H-I)** Dot plots unsorted and VGLUT1^{venus} + sorted synaptosomes stained for VGLUT1 and VGLUT2. and galleries of representative epifluorescence images. Note the low representation of synaptosomes associating VGLUT1 (cortico-striatal inputs) and VGLUT2 (Thalamo-striatal inputs). Indeed VGLUT1/-2 double positives do not enrich through FASS. **(J)** Dot plot of intensity signal of unsorted synaptosomes stained for the inhibitory post-synaptic scaffold protein gephyrin and the inhibitory presynaptic marker VIAAT. Galleries of representative epifluorescence images of analyzed particles. Surprisingly the pre/postsynaptic association is not maintained at individual inhibitory sucrose synaptosomes. Scale bars 1 μm.

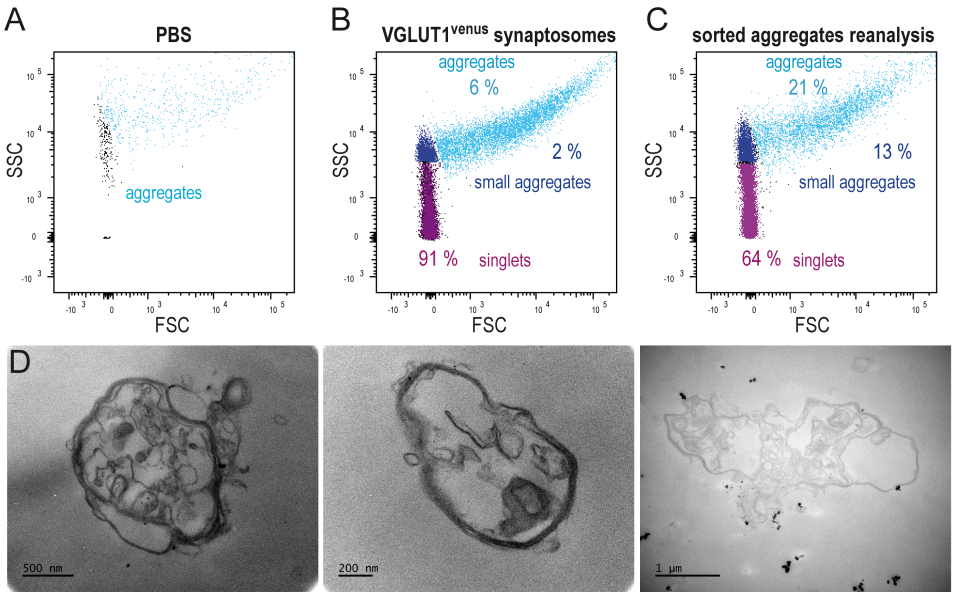

Figure S4: Sorted aggregates do not display hub synaptosome like shapes. (A-D) Representative FASS gating for aggregates sorting. **(A)** Analysis of PBS was used to define background noise. The noise was less than 500 events per minute. **(B)** Sucrose VGLUT1^{venus} synaptosome samples showed 6% of aggregated particles (light blue). **(C)** Particles gated as "aggregates" were sorted and reanalyzed. Small and large aggregates represented 34% of particles after sorting. Indeed unspecific aggregates tend to break down upon the shearing forces of the FACS and generates singlets at reanalysis. **(D)** Electron micrographs of sorted aggregated particles. Aggregates appear much larger than hub synapses. Their cellular content is difficult to identify though myelin membranes may be recognized on some of them. Scale bar, 500nm, 200nm, 1µm (from left to right).